CrossMark

ORIGINAL PAPER

# [F-18]-AV-1451 binding correlates with postmortem neurofibrillary tangle Braak staging

Marta Marquié[1,2] · Michael Siao Tick Chong[1,2] · Alejandro Antón-Fernández[1,2] · Eline E. Verwer[3] ·
Nil Sáez-Calveras[1,2] · Avery C. Meltzer[1,2] · Prianca Ramanan[1,2] · Ana C. Amaral[1,2] · Jose Gonzalez[1,2,4] ·
Marc D. Normandin[3] · Matthew P. Frosch[1,2,4] · Teresa Gómez-Isla[1,2]

**Abstract** [F-18]-AV-1451, a PET tracer specifically developed to detect brain neurofibrillary tau pathology, has the potential to facilitate accurate diagnosis of Alzheimer's disease (AD), staging of brain tau burden and monitoring disease progression. Recent PET studies show that patients with mild cognitive impairment and AD dementia exhibit significantly higher in vivo [F-18]-AV-1451 retention than cognitively normal controls. Importantly, PET patterns of [F-18]-AV-1451 correlate well with disease severity and seem to match the predicted topographic Braak staging of neurofibrillary tangles (NFTs) in AD, although this awaits confirmation. We studied the correlation of autoradiographic binding patterns of [F-18]-AV-1451 and the stereotypical spatiotemporal pattern of progression of NFTs using legacy postmortem brain samples representing different Braak NFT stages (I-VI). We performed [F-18]-AV-1451 phosphor-screen autoradiography and quantitative tau measurements (stereologically based NFT counts and biochemical analysis of tau pathology) in three brain regions (entorhinal cortex, superior temporal sulcus and visual cortex) in a total of 22 cases: low Braak (I–II, $n = 6$), intermediate Braak (III–IV, $n = 7$) and high Braak (V–VI, $n = 9$).

Strong and selective [F-18]-AV-1451 binding was detected in all tangle-containing regions matching precisely the observed pattern of PHF-tau immunostaining across the different Braak stages. As expected, no signal was detected in the white matter or other non-tangle containing regions. Quantification of [F-18]-AV-1451 binding was very significantly correlated with the number of NFTs present in each brain region and with the total tau and phospho-tau content as reported by Western blot and ELISA. [F-18]-AV-1451 is a promising biomarker for in vivo quantification of brain tau burden in AD. Neuroimaging–pathologic studies conducted on postmortem material from individuals imaged while alive are now needed to confirm these observations.

**Keywords** [F-18]-AV-1451 · PET · Tau · Neurofibrillary tangles · Braak staging · Alzheimer

✉ Teresa Gómez-Isla
tgomezisla@partners.org

1    MassGeneral Institute for NeuroDegenerative Disease, Charlestown, MA, USA

2    Department of Neurology, Massachusetts General Hospital, WACC Suite 715., 15th Parkman St., Boston, MA 02114, USA

3    Department of Radiology, Gordon Center for Medical Imaging, Massachusetts General Hospital, Boston, MA, USA

4    C.S. Kubik Laboratory for Neuropathology, Massachusetts General Hospital, Boston, MA, USA

## Introduction

Novel positron emission tomography (PET) tau tracer [F-18]-AV-1451 is a promising tool for the in vivo diagnosis and monitoring of patients with Alzheimer's disease (AD) [5, 34]. We and others have previously shown that [F-18]-AV-1451 binds with strong affinity to paired helical filament (PHF)-tau aggregates in AD brains and those that form as a function of age [12–14, 26, 34]. In agreement with these observations, patients clinically diagnosed with dementia of AD type and mild cognitive impairment (MCI) exhibit significantly higher in vivo [F-18]-AV-1451 retention than cognitively normal individuals in regions that are known to contain an elevated burden of tau lesions in AD [3, 6–8, 10, 21, 27, 33].

Neurofibrillary pathology (neurofibrillary tangles (NFTs) and neuropil threads) in AD brains follows a

stereotypical spatiotemporal progression that was initially described by Braak and Braak and categorized into six stages that can be summarized in three: entorhinal (stages I–II), limbic (stages III–IV), and isocortical (stages V–VI) [2]. The first NFTs appear in the transentorhinal region (stage I) along with the entorhinal cortex, followed by the CA1 region of the hippocampus (stage II). Next, NFTs develop in limbic structures such as the subiculum (stage III), followed by the amygdala, thalamus and claustrum (stage IV). Finally, NFTs spread to all isocortical areas, with the neocortical association areas being affected prior and more severely (stage V) than primary motor, sensory, and visual areas (stage VI). In general, the accumulation and spreading of tau lesions through increasing Braak stages parallels the progression and severity of clinical symptoms of the disease. Braak stages I–II do not present with any cognitive impairment, mild cognitive deficits typically emerge as tau pathology advances towards limbic regions (Braak stages III–IV), and a fully developed clinical picture of dementia is present in most cases once tau lesions have reached neocortical association areas (Braak stages V–VI) [19, 23, 29].

Several recent studies suggest that in vivo [F-18]-AV-1451 retention patterns in cognitively normal individuals and patients with MCI and AD dementia match the predicted topographic Braak staging of NFTs [6, 27, 28, 33]. This points to the potential usefulness of this tracer as an in vivo surrogate marker to estimate brain tau burden in AD patients, and to track disease progression in very mildly impaired individuals who are suspected to harbor AD pathology in their brains. Importantly, the combination of [F-18]-AV-1451 imaging with other AD biomarkers such as PET amyloid tracers [25, 31] and CSF measurements of total-tau, phospho-tau and Aβ [15, 24] is expected to increase further the diagnostic accuracy across the spectrum of normal aging, MCI and AD.

In the present study we have analyzed postmortem human brain tissue samples from 22 cases representing the spectrum of NFT Braak staging, from Braak stages I–II to VI. Binding of [F-18]-AV-1451 in three different brain regions (entorhinal cortex (EC), the cortex lining the superior temporal sulcus (STS), and visual cortex (VC)) was assessed by phosphor-screen autoradiography and compared to quantitative tau measurements (stereologically based NFT counts and biochemical analysis of tau pathology) in those same regions. Our data show that [F-18]-AV-1451 binding correlates very closely with the number of NFTs and with synaptic total-tau and phosphorylated tau content as assessed by Western Blot (WB) and Enzyme-like immunosorbent assay (ELISA). These findings support the idea that [F-18]-AV-1451 is a promising surrogate marker for quantification and staging of pathological tau burden in AD; something that may

prove essential for evaluating disease progression and for assessing response to tau-targeted therapies.

## Materials and methods

### Brain tissue samples

Twenty-two cases representative of the spectrum of Braak NFT staging (I–VI) [1, 2] from the Massachusetts Alzheimer's Disease Research Center (MADRC) Neuropathology Core were included in this study. Cases were selected based on the availability of enough frozen tissue in each region of interest to perform the experiments detailed below. Postmortem brain samples were processed and analyzed at the MADRC Neuropathology Core. Autopsies were performed according to standardized protocols [32], and tissue collection and use were approved by the local Institutional Review Board. Diagnostic evaluation was performed in accordance with published guidelines for neurodegenerative diseases [4, 9, 16]. All cases were reviewed by a board certified neuropathologist. Braak staging for NFT deposition [2] and Consortium to Establish a Registry for Alzheimer's disease (CERAD) score for neuritic amyloid plaques [18] were reviewed in each case.

Cases were classified into three categories according to their Braak NFT stage [1, 2]: low Braak (Braak stages I–II, $n = 6$), intermediate Braak (Braak stages III–IV, $n = 7$) and high Braak (Braak stages V–VI, $n = 9$). Three brain regions were selected for the analysis: EC, the multimodal association cortex lining the STS, and VC. Blocks of frozen brain tissue containing each of the three regions of interest, respectively, were sectioned in a cryostat (Thermo-Shandon SME Cryostat) into 10-μm-thick slices and used for immunohistochemistry (IHC) and phosphor-screen autoradiography. Fresh frozen homogenates prepared from the same tissue material were used to quantify tau content by WB and ELISA.

### [F-18]-AV-1451 phosphor-screen autoradiography

[F-18]-AV-1451 phosphor-screen autoradiography was performed following the protocol that we have previously described in detail elsewhere [14]. ImageJ (National Institute of Health, NIH) was used to quantify the [F-18]-AV-1451 signal in the three regions of interest (EC, STS and VC). Digital images of each slide were obtained, background subtraction was applied, and the mean signal in each region of interest was calculated by densitometry.

## Pathological tau burden quantification by immunohistochemistry

Ten-micrometer-thick frozen tissue sections adjacent to those used in autoradiographic experiments were stained with PHF-1 antibody (1:100 dilution, mouse, kind gift of Dr. Peter Davies) to visualize NFTs. Samples were then analyzed with an upright Olympus BX51 microscope (Olympus, Denmark) using the CAST software (Visiopharm, 2004, Denmark). Each region of interest was drawn in the corresponding slide at 1.25× magnification, and then randomly sampled using the software's optical dissector probe at 10× magnification (meander sampling 20%, counting frame 10%, dissector size 238.4 μm × 239.3 μm). The number of NFTs present inside each dissector was annotated; the total number of NFTs in each region of interest was then calculated using the following formula: (total number of NFT counted/sum of the areas of all the dissectors) × 10 μm.

## β-Amyloid plaque burden quantification by immunohistochemistry

Ten-micrometer-thick frozen tissue sections adjacent to those used for tau immunohistochemistry and autoradiography were stained with an anti-Aβ antibody (Amyloid β (N) Anti-Human Rabbit IgG Affinity Purify, 1:500 dilution, IBL International). The samples were analyzed with an upright Olympus BX51 microscope (Olympus, Denmark) using the CAST software (Visiopharm, 2004, Denmark). Each region of interest was drawn in the corresponding section at 1.25× magnification and randomly sampled using the software's optical dissector probe at 10× magnification (meander sampling 20%). A threshold of optical density was obtained in each photomicrograph using ImageJ (NIH). Manual editing in each field eliminated artifacts. Amyloid-β plaque burden, defined as total percentage (%) of area covered by Aβ immunostained plaques, was calculated in each region of interest.

## Analysis of tau content by Western Blot and ELISA

Synaptoneurosomal, cytosolic, and total fractions from the three regions of interest (EC, STS and VC) were obtained by homogenizing tissue in Buffer A (25 mM HEPES 7.5, 120 mM NaCl, 5 mM KCL, 1 mM $MgCl_2$, 2 mM $CaCl_2$, 1 mM DTT) supplemented with Phosphatase Inhibitor Cocktail tablets (Roche, 04906845001) and Protease Inhibitor Cocktail tablets (Roche, 11697498001). The homogenate was filtered through 2 Millipore Nylon 80 μm filters after the addition of 0.6 mL Buffer A and 200 μL of homogenate was separated. 200μL of distilled $H_2O$ and 70 μL of 10% SDS were added to the homogenate

and passed through a 27½G needle 3 times. The remaining homogenate was filtered again through PALL Acrodisc Syringe 5 μm Filters after the addition of 1 mL Buffer A, and centrifuged at 1000$g$ for 10 min at 4 °C. The supernatant was then separated and ultracentrifuged at 100,000$g$ for 45 min, and the pellet was resuspended in 200 μL Buffer B (50 mM Tris, 1.5% SDS, 1 mM DTT). The resuspended pellet and the separated homogenate were then boiled for 5 min, centrifuged for 15 min, and the supernatants were collected as synaptoneurosome (SNS) and total fractions, respectively. The supernatant of the ultracentrifuged samples were collected as the cytosolic fraction.

SNS fractions from each region of interest were electrophoresed in MES SDS Running Buffer (Novex, NP0002) using 4–12% Bis–Tris Novex gels (Invitrogen, #MAN0003679). Protein was then transferred onto nitrocellulose membranes and blocked for an hour at room temperature using Odyssey Blocking Buffer (LiCor, 927-40000). Membranes were probed with human tau (Dako, A0024) and PHF-1 (kind gift of Dr. Peter Davies) antibodies to detect content of total tau and phospho-tau, respectively. GAPDH (Millipore, AB2302) was used as loading control for protein normalization. LiCor secondary antibodies (IR Dye 680RD Donkey anti-chicken 926-68075, IR Dye 800 CW Donkey anti-rabbit 926-32213, IR Dye 800CW Donkey anti-mouse 926-32212) were then used to visualize bands with the Odyssey Infrared Imaging System (V3.0). ImageStudio was used to quantify the bands of interest by drawing equal size rectangles around individual bands of interest. Background subtraction was applied by taking the median of the area three pixels to the left and right of each band of interest and subtracting that value from the measured signal.

SNS content of phosphorylated-tau was also measured by ELISA using the solid phase Human Tau (pS396) ELISA Kit (Invitrogen, KHB7031) following the manufacturer's instructions. In brief, SNS fractions were added to human Tau monoclonal antibody coated 96 well plates. Captured phosphorylated tau was detected using Human Tau (pS396) Detection Antibody and Anti-Rabbit IgG HRP. Absorbance values were measured at 450 nm using a plate reader (Wallac 1420 VICTOR2, Perkin Elmer). All samples were run in duplicates.

## Statistical analysis

Correlations between [F-18]-AV-1451 autoradiography densitometry, PHF-tau and Aβ burden quantifications by IHC, and quantifications of tau contents by ELISA and WB were performed using a linear regression test. Significance was set at $p < 0.05$. All statistical analysis and graphs were generated using GraphPad Prism v6.0 software (GraphPad Software Inc., La Jolla, CA, USA).

## Results

A summary of the demographic and neuropathological features of the 22 subjects studied are shown in Table 1. The age range in this series was 59–101, 64% of subjects (n = 14) were female, and all of them were Caucasian. Subjects were classified according to their NFT Braak staging [2] into three categories: low Braak (Braak stages I–II, n = 6), intermediate Braak (Braak stages III–IV, n = 7) and high Braak (Braak stages V–VI, n = 9).
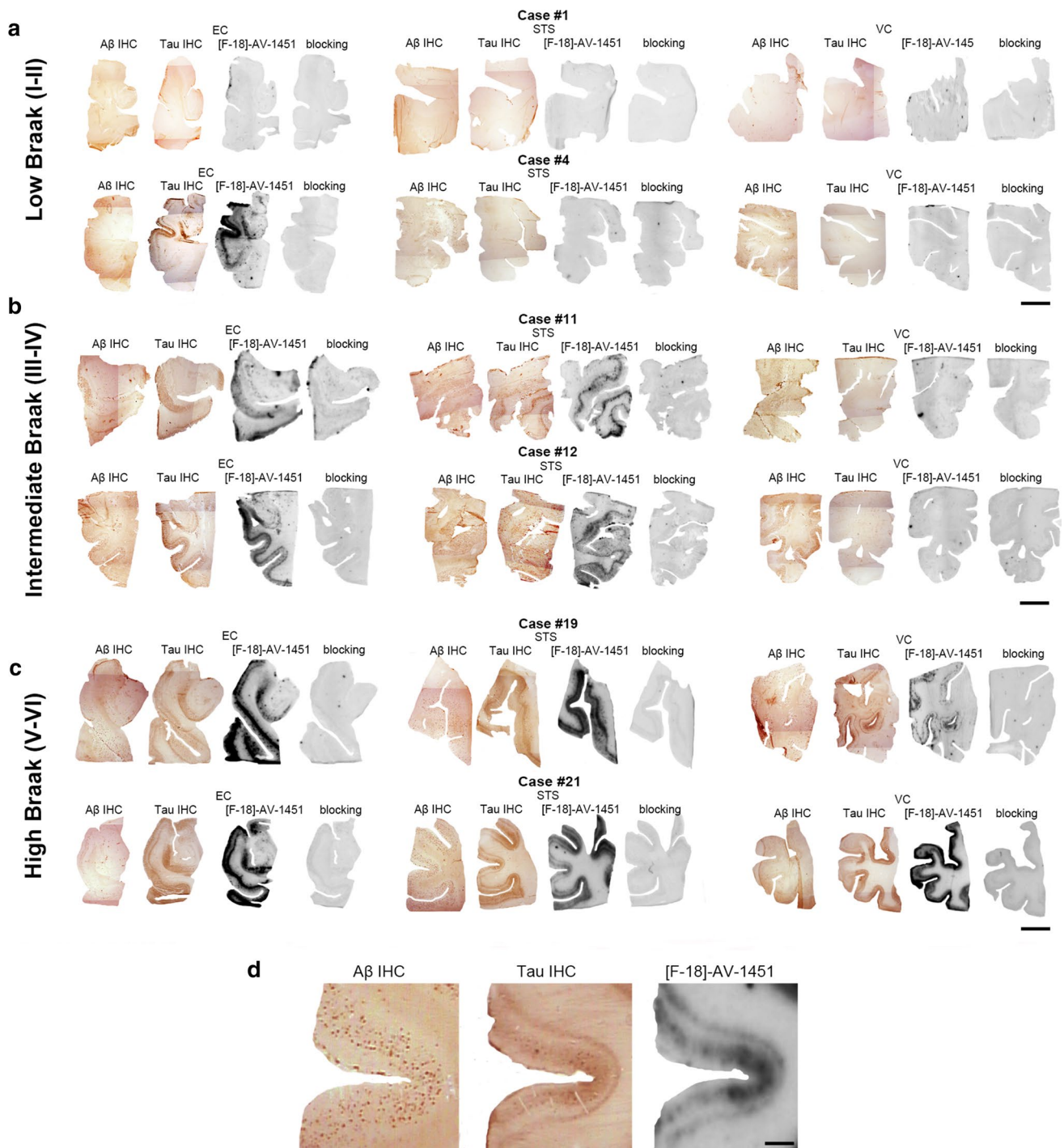
## [F-18]-AV-1451 phosphor-screen autoradiography

Phosphor-screen autoradiography was performed on brain tissue slides containing the three regions of interest: EC, STS and VC. Strong and selective [F-18]-AV-1451 binding was detected in all tangle-containing regions matching precisely the observed pattern of PHF-tau immunostaining corresponding to the different Braak stages (Fig. 1). Individuals in the low Braak category (stages I–II) (Fig. 1a) showed [F-18]-AV-1451 binding exclusively in EC; intermediate

**Table 1** Demographic and neuropathologic information from the study subjects

| dID | Age at death (years) | Gender (M/F) | Braak stage (NFT) | CERAD score (neuritic plaque) | Thal phase (amyloid) | Other neuropathological findings |
|---|---|---|---|---|---|---|
| Low Braak stage | | | | | | |
| #1 | 81 | M | I | None | 1 | Severe arteriosclerosis, hippocampal sclerosis, right cerebellar infarct |
| #2 | 76 | F | I | Sparse | 2 | Mild CAA, hypoxic/ischemic injury |
| #3 | 97 | F | I | Sparse | 1 | Severe hypertensive white matter cerebrovascular disease, falcine meningioma |
| #4 | 101 | F | II | Moderate | 2 | Severe hypertensive cerebrovascular disease. Acute occipital infarct |
| #5 | 59 | F | II | Moderate | 2 | Motor cortex microinfarct |
| #6 | 91 | M | II | Sparse | 0 | Moderate arteriosclerosis |
| Intermediate Braak stage | | | | | | |
| #7 | 94 | M | III | Sparse | 3 | Severe arteriolosclerosis, mild CAA, old micro-infarcts |
| #8 | 91 | F | III | Sparse | 3 | Severe atherosclerosis |
| #9 | 87 | M | III | None | 1 | Moderate hypertensive cerebrovascular disease |
| #10 | 91 | M | III | Sparse | 1 | Moderate arteriolosclerosis, mild CAA |
| #11 | 78 | F | IV | Frequent | 2 | Mild CAA, hypertensive cerebrovascular disease |
| #12 | 86 | F | IV | Moderate | 5 | TDP43 inclusions in medial temporal lobe, mild CAA, moderate arteriolosclerosis |
| #13 | 87 | F | IV | Sparse | 4 | ALS-TDP43 proteinopathy, mild CAA, moderate arteriolosclerosis |
| High Braak stage | | | | | | |
| #14 | 87 | F | V | Moderate | 3 | Moderate arteriosclerosis, mild CAA, old micro-infarct in superior parietal cortex |
| #15 | 71 | M | V | Moderate | 4 | Mild CAA, moderate hypertensive cerebrovascular disease |
| #16 | 96 | F | V | Frequent | 2 | N/A |
| #17 | 82 | F | V | Moderate | 4 | Mild CAA, mild arteriolosclerosis |
| #18 | 79 | M | V | Frequent | 5 | Moderate hypertensive cerebrovascular disease |
| #19 | 66 | M | V | Moderate | 4 | Moderate CAA, right motor cortex microinfarct, moderate arteriolosclerosis |
| #20 | 69 | F | VI | Frequent | 5 | Mild CAA |
| #21 | 66 | F | VI | Frequent | 4 | Moderate arteriolosclerosis |
| #22 | 66 | F | VI | Frequent | 5 | Moderate hypertensive cerebrovascular disease, mild CAA |

*ALS* amyotrophic lateral sclerosis, *CAA* cerebral amyloid angiopathy, *CERAD* Consortium to establish a Registry for Alzheimer's disease, *CTL* control, *F* female, *M* male, *N/A* not available, *NFT* neurofibrillary tangles

**Fig. 1** Microphotographs of postmortem brain tissue sections depicting Aβ and PHF-1 tau immunostaining, [F-18]-AV-1451 phosphorscreen autoradiography and blocking conditions in adjacent slides from representative subjects at different Braak stages [2]: **a** low Braak, **b** intermediate Braak, and **c** high Braak, and high magnification microphotographs depicting Aβ and PHF-1 tau immunostaining and [F-18]-AV-1451 phosphor-screen autoradiography of the STS from case #21 (**d**). [F-18]-AV-1451 binding was detected in all tangle-containing regions matching the pattern of PHF-tau immunostaining across the different Braak stages, but not the Aβ immunosignal. No [F-18]-AV-1451 binding was detected in white matter or in cortical regions lacking NFTs. *Scale bar* 1 cm (**a–c**), 2 mm (**d**). *Aβ* β-amyloid, *IHC* immunohistochemistry, *NFT* neurofibrillary tangles, *PHF* paired helical filament
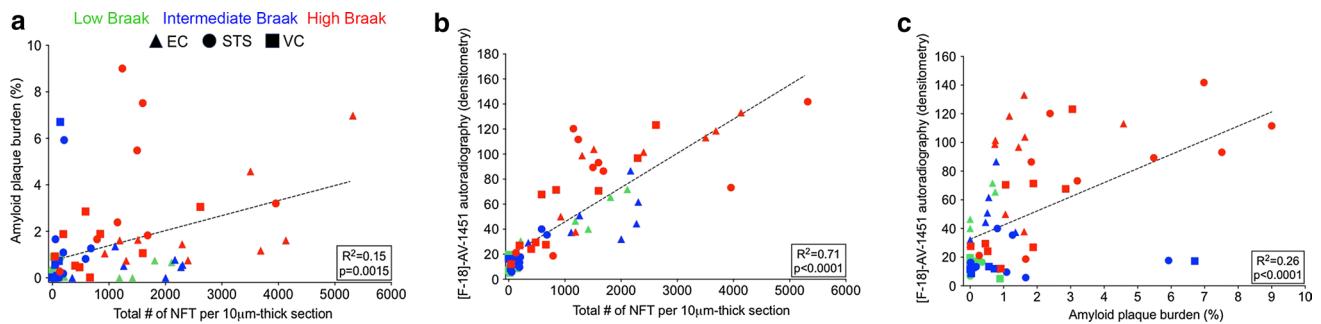
**Fig. 2** A significant correlation was detected between Aβ plaque burden and total number of NFTs per 10 μm-thick section ($R^2 = 0.15$, $p = 0.0015$) (**a**). [F-18]-AV-1451 autoradiography signal significantly correlated with total number of NFTs per 10 μm-thick section ($R^2 = 0.71$, $p < 0.0001$) (**b**), and Aβ plaque load ($R^2 = 0.26$, $p < 0.0001$) (**c**). *Aβ* β-amyloid, *EC* entorhinal cortex, *IHC* immunohistochemistry, *NFT* neurofibrillary tangles, *STS* superior temporal sulcus, *VC* visual cortex, *PHF* paired helical filament

Braak cases (stages III–IV) (Fig. 1b) exhibited tracer binding in EC and STS; and high Braak cases (stages V–VI) (Fig. 1c) showed binding in all three ROIs. Of note, binding was almost completely blocked after incubating the slides with 1 μM unlabeled AV-1451, demonstrating the specificity of the signal. As expected, no signal was detected in the white matter or in non-tangle containing regions in any of the three slides examined. Consistent with our previously reported observations [14], the distribution of the autoradiographic [F-18]-AV-1451 binding closely mirrored the pattern of PHF-1 immunostaining reactivity on adjacent slices with the highest amount of signal being observed in cortical layers III and V, as expected based on the well-known robust density of tangle lesions in those cortical layers, as opposed to the more scattered plaque distribution pattern revealed by Aβ immunostaining (Fig. 1d). Our previous studies using a fine grain nuclear photographic emulsion and immunohistochemistry to obtain resolution at the cellular level, demonstrated that [F-18]-AV-1451 selectively binds to PHF-tau containing lesions, including NFTs (intra and extraneuronal) and PHF-tau containing neurites, but does not bind to Aβ plaques or amyloid-laden vessels [14].

## Correlation of Tau and Aβ-plaque burden with [F-18]-AV-1451 binding

Total number of NFTs per 10 μm section was significantly, but weakly, correlated with Aβ-plaque load when all three regions of interest (EC, STS and VC) and Braak stages were included in the analysis ($R^2 = 0.15$, $p = 0.0015$; Fig. 2a). In general, and not surprisingly, cases with high Braak NFT stages (V–VI) also exhibited a higher Aβ-plaque burden in the regions analyzed. Autoradiographic [F-18]-AV-1451

binding correlated strongly with total number of NFTs ($R^2 = 0.71$, $p < 0.0001$; Fig. 2b) and significantly, but weakly, with Aβ-plaque load ($R^2 = 0.26$, $p < 0.0001$) (Fig. 2c).

## Correlation of total tau and phosphorylated-tau content by Western blot and [F-18]-AV-1451 autoradiographic binding

Analysis of SNS fractions by WB revealed the presence of tau in the form of low molecular weight (monomeric) and high molecular weight (oligomeric) species. Representative images of total tau and phosphorylated tau species in different regions of interest, as reported by WB, are shown in Fig. 3a, c. As expected, levels of total tau and phosphorylated tau, particularly in the form of oligomeric species, were substantially higher in high Braak stage cases (V–VI). A very significant correlation was detected between autoradiographic [F-18]-AV-1451 binding and the content of monomeric and oligomeric total tau ($R^2 = 0.50$, $p < 0.0001$ and $R^2 = 0.72$, $p < 0.0001$, respectively; Fig. 3b) and phospho-tau in SNS fractions ($R^2 = 0.80$, $p < 0.0001$ and $R^2 = 0.76$, $p < 0.001$, respectively; Fig. 3d).

## Correlation of phosphorylated-tau content by ELISA and [F-18]-AV-1451 autoradiographic binding

Analysis of the content of phosphorylated tau in SNS fractions by sensitive ELISA further confirmed the strong and significant correlation of autoradiographic [F-18]-AV-1451 binding with levels of phosphorylated tau species aberrantly accumulated in the synaptic compartment in this series ($R^2 = 0.76$, $p < 0.0001$; Fig. 3e).
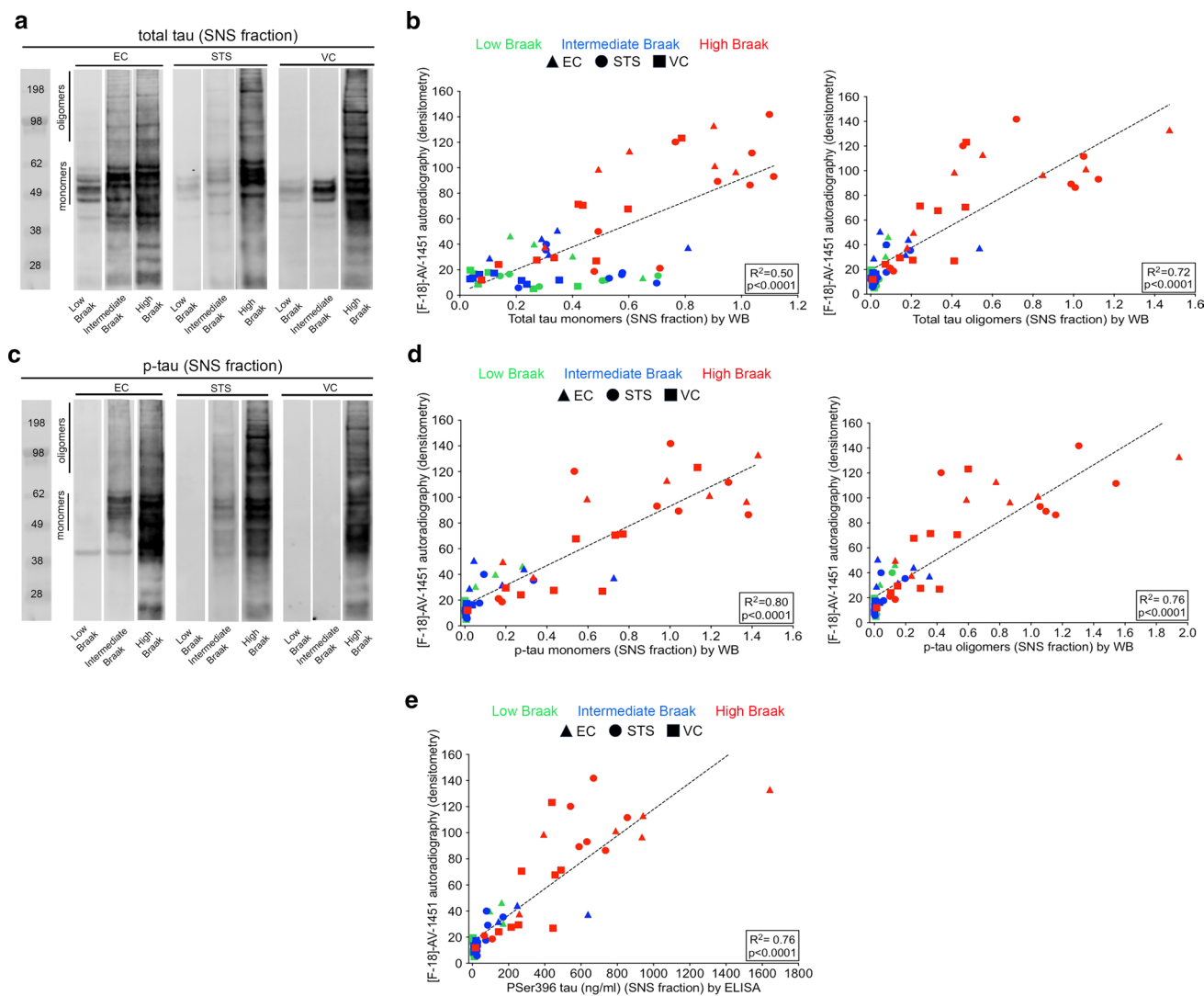
**Fig. 3** Biochemical analysis of total tau and phosphorylated tau (monomeric and oligomeric) species in the SNS compartment by WB (**a–d**) and of Pser396 tau by ELISA (**e**). Representative images of total tau (**a**) and phosphorylated tau (**c**) content in SNS fractions by WB and across different Braak stages [2] in EC, STS and VC cortex are shown for comparison. A significant correlation was observed between [F-18]-AV-1451 autoradiographic binding and levels of monomeric and oligomeric tau ($R^2 = 0.50$, $p < 0.0001$ and $R^2 = 0.72$, $p < 0.0001$, respectively) (**b**), and monomeric and oligomeric phos-phorylated tau ($R^2 = 0.80$, $p < 0.0001$ and $R^2 = 0.76$, $p < 0.001$, respectively) (**d**). A significant correlation was also observed between [F-18]-AV-1451 autoradiography binding and pSer396 tau levels in the SNS fraction as measured by ELISA ($R^2 = 0.76$, $p < 0.0001$) (**e**). *EC* entorhinal cortex, *ELISA* enzyme-like immunosorbent assay, *NFT* neurofibrillary tangle, *p-tau* hyperphosphorylated tau, *SNS* synaptoneurosome, *STS* superior temporal sulcus, *VC* visual cortex, *WB* western blot

## Discussion

We have evaluated the potential usefulness of novel tau PET tracer [F-18]-AV-1451 to quantify pathological tau burden and track the stereotypical spatiotemporal progression of NFT pathology in the human AD brain. Our observations are derived from [F-18]-AV-1451 autoradiography, detailed stereologically based counts of NFTs and quantification of Aβ-plaque burden on immunostained sections, and biochemical analysis of tau content by WB and ELISA in 22 autopsied brains representing the entire spectrum of

AD progression (Braak NFT staging), from Braak stages I–II (entorhinal) to stages V–VI (isocortical). Our data indicate that [F-18]-AV-1451 binding faithfully correlates with the distribution and progressive accumulation of NFTs and the aberrant accrual of tau species in synapses that characterize the different stages of AD progression. Altogether our findings suggest that this tau PET tracer holds promise for the in vivo estimation of pathological tau burden and Braak staging.

Our previous observations suggested that [F-18]-AV-1451 exhibits high binding affinity for tau

aggregates in the form of NFTs and paired helical filament-tau-containing neurites in AD but does not bind to a significant extent to tau inclusions mainly made of straight tau filaments in non-AD tauopathies [13, 14], although the latter remains controversial [11, 17, 30]. Importantly, we observed a robust off-target binding of AV-1451 to neuromelanin- and melanin-containing cells; a finding that has proven very relevant for the accurate interpretation of [F-18]-AV-1451 in vivo retention patterns. Other authors have made similar observations [12, 26, 34]. Accordingly, in vivo imaging studies have shown that patients clinically diagnosed with MCI and AD dementia exhibit significantly higher retention of this tracer in brain regions that are expected to harbor neurofibrillary tau pathology when compared to aged-matched cognitively normal subjects [10]. Of note, emerging data also suggest that the in vivo retention patterns of [F-18]-AV-1451 correlate with clinical disease severity and seem to match the predicted topographic Braak staging of NFTs in AD [27, 28, 33]. It is now crucial to confirm these observations. In the present study, we have taken a first step to demonstrate that [F-18]-AV-1451 can serve as a surrogate biomarker for accurately quantifying tau burden and tracking the progression of AD over time (Braak staging) in the human living brain.

Taking advantage of the large collection of well-characterized legacy postmortem tissue samples in our MADRC Neuropathology Core, we selected a series of 22 brains from subjects representing the entire spectrum of Braak staging [2]. We selected blocks containing three brain regions (EC, the cortex lining the STS and the VC) to illustrate the progressive accumulation and predicted spreading of NFTs from transentorhinal/entorhinal cortices to limbic structures and isocortical areas. Our results from phosphor-screen autoradiography confirmed that [F-18]-AV-1451 avidly bound to PHF-tangle containing slices demonstrating very low nonspecific binding to the whiter matter. [F-18]-AV-1451 binding was confined to the EC in cases with low Braak stage (I–II) reflecting the presence of incidental age-related NTFs in these subjects, progressing to the STS in subjects with intermediate Braak stage (III–IV), and extending to the VC in subjects with high Braak stage (V–VI). In agreement with our previous observations [14], the laminar autoradiographic pattern of distribution of [F-18]-AV-1451 revealed a strong labeling in particular of layers III and V, matching the preferential laminar distribution of NFTs on adjacent immunostained sections. These data strongly suggest that [F-18]-AV-1451 is a very promising surrogate marker for estimating in vivo Braak staging; something that may prove to have important practical implications. As it has been recently suggested, knowledge of the in vivo Braak staging using tau PET imaging could be particularly valuable to stratify participants in clinical trials into more homogeneous groups, improving the power of the trial and reducing the required sample size [22]. It could also be useful in helping patients and caregivers understand the likely rate of disease progression over time and develop a plan of care.

Importantly, [F-18]-AV-1451 binding not only precisely matched the regional pattern of distribution of NFTs in the different Braak stages, but also very closely correlated with stereologically based counts of total number of NFTs and with synaptic content of total tau and phosphorylated tau species, as reported by WB and sensitive ELISA, in the regions of interest. Of note, we have recently reported that aberrant accrual of oligomeric phosphorylated tau species in the synaptic compartment is a very proximate correlate to cognition and neuronal cell loss in AD [20]. These findings further suggest that [F-18]-AV-1451 may not only allow in vivo Braak staging but also a reliable quantification of the pathological tau load; something that may be especially valuable for assessing the response to tau-targeted therapies.

In conclusion, our results suggest that [F-18]-AV-1451 holds great promise as a surrogate marker for the in vivo quantification and staging of tau pathology in AD brains. Future imaging-pathological correlation studies conducted on material from individuals scanned while alive at different stages will provide additional information for the reliable interpretation of change of tau pathology burden in AD and its relationship with clinical progression of the disease, and for the potential use of this PET tracer to test interventions aimed at decreasing NFT burden or halting spreading of tau pathology.

**Compliance with ethical standards**

**Ethical approval** All procedures performed in studies involving human participants were in accordance with the ethical standards of the institutional and national research committee and with the 1964 Helsinki declaration and its later amendments.

**Informed consent** Informed consent was obtained from all individual participants included in the study.

# References

1. Braak H, Alafuzoff I, Arzberger T, Kretzschmar H, Del Tredici K (2006) Staging of Alzheimer disease-associated neurofibrillary pathology using paraffin sections and immunocytochemistry. Acta Neuropathol 112:389–404. doi:10.1007/s00401-006-0127-z

2. Braak H, Braak E (1991) Neuropathological stageing of Alzheimer-related changes. Acta Neuropathol 82:239–259

3. Brier MR, Gordon B, Friedrichsen K, McCarthy J, Stern A, Christensen J, Owen C, Aldea P, Su Y, Hassenstab J et al (2016) Tau and Abeta imaging, CSF measures, and cognition in Alzheimer's disease. Sci Transl Med 8:338ra366. doi:10.1126/scitranslmed.aaf2362

4. Cairns NJ, Bigio EH, Mackenzie IR, Neumann M, Lee VM, Hatanpaa KJ, White CL 3rd, Schneider JA, Grinberg LT, Halliday G et al (2007) Neuropathologic diagnostic and nosologic criteria for frontotemporal lobar degeneration: consensus of the Consortium for Frontotemporal Lobar Degeneration. Acta Neuropathol 114:5–22. doi:10.1007/s00401-007-0237-2

5. Chien DT, Bahri S, Szardenings AK, Walsh JC, Mu F, Su MY, Shankle WR, Elizarov A, Kolb HC (2013) Early clinical PET imaging results with the novel PHF-tau radioligand [F-18]-T807. J Alzheimer's Dis JAD 34:457–468. doi:10.3233/JAD-122059

6. Cho H, Choi JY, Hwang MS, Kim YJ, Lee HM, Lee HS, Lee JH, Ryu YH, Lee MS, Lyoo CH (2016) In vivo cortical spreading pattern of tau and amyloid in the Alzheimer disease spectrum. Ann Neurol 80:247–258. doi:10.1002/ana.24711

7. Cho H, Choi JY, Hwang MS, Lee JH, Kim YJ, Lee HM, Lyoo CH, Ryu YH, Lee MS (2016) Tau PET in Alzheimer disease and mild cognitive impairment. Neurology 87:375–383. doi:10.1212/WNL.0000000000002892

8. Gordon BA, Friedrichsen K, Brier M, Blazey T, Su Y, Christensen J, Aldea P, McConathy J, Holtzman DM, Cairns NJ et al (2016) The relationship between cerebrospinal fluid markers of Alzheimer pathology and positron emission tomography tau imaging. Brain J Neurol 139:2249–2260. doi:10.1093/brain/aww139

9. Hyman BT, Phelps CH, Beach TG, Bigio EH, Cairns NJ, Carrillo MC, Dickson DW, Duyckaerts C, Frosch MP, Masliah E et al (2012) National Institute on Aging-Alzheimer's Association guidelines for the neuropathologic assessment of Alzheimer's disease. Alzheimer's Dement J Alzheimer's Assoc 8:1–13. doi:10.1016/j.jalz.2011.10.007

10. Johnson KA, Schultz A, Betensky RA, Becker JA, Sepulcre J, Rentz D, Mormino E, Chhatwal J, Amariglio R, Papp K et al (2016) Tau positron emission tomographic imaging in aging and early Alzheimer disease. Ann Neurol 79:110–119. doi:10.1002/ana.24546

11. Josephs KA, Whitwell JL, Tacik P, Duffy JR, Senjem ML, Tosakulwong N, Jack CR, Lowe V, Dickson DW, Murray ME (2016) [18F]AV-1451 tau-PET uptake does correlate with quantitatively measured 4R-tau burden in autopsy-confirmed corticobasal degeneration. Acta Neuropathol 132:931–933. doi:10.1007/s00401-016-1618-1

12. Lowe VJ, Curran G, Fang P, Liesinger AM, Josephs KA, Parisi JE, Kantarci K, Boeve BF, Pandey MK, Bruinsma T et al (2016) An autoradiographic evaluation of AV-1451 Tau PET in dementia. Acta Neuropathol Commun 4:58. doi:10.1186/s40478-016-0315-6

13. Marquie M, Normandin MD, Meltzer AC, Siao Tick Chong M, Andrea NV, Anton-Fernandez A, Klunk WE, Mathis CA, Ikonomovic MD, Debnath M et al (2017) Pathological correlations of [F-18]-AV-1451 imaging in non-alzheimer tauopathies. Ann Neurol 81:117–128. doi:10.1002/ana.24844

14. Marquie M, Normandin MD, Vanderburg CR, Costantino IM, Bien EA, Rycyna LG, Klunk WE, Mathis CA, Ikonomovic MD, Debnath ML et al (2015) Validating novel tau positron emission tomography tracer [F-18]-AV-1451 (T807) on postmortem brain tissue. Ann Neurol 78:787–800. doi:10.1002/ana.24517

15. Mattsson N, Rosen E, Hansson O, Andreasen N, Parnetti L, Jonsson M, Herukka SK, van der Flier WM, Blankenstein MA, Ewers M et al (2012) Age and diagnostic performance of Alzheimer disease CSF biomarkers. Neurology 78:468–476. doi:10.1212/WNL.0b013e3182477eed

16. McKeith IG (2006) Consensus guidelines for the clinical and pathologic diagnosis of dementia with Lewy bodies (DLB): report of the Consortium on DLB International Workshop. J Alzheimer's Dis JAD 9:417–423

17. McMillan CT, Irwin DJ, Nasrallah I, Phillips JS, Spindler M, Rascovsky K, Ternes K, Jester C, Wolk DA, Kwong LK et al (2016) Multimodal evaluation demonstrates in vivo 18F-AV-1451 uptake in autopsy-confirmed corticobasal degeneration. Acta Neuropathol 132:935–937. doi:10.1007/s00401-016-1640-3

18. Mirra SS, Heyman A, McKeel D, Sumi SM, Crain BJ, Brownlee LM, Vogel FS, Hughes JP, van Belle G, Berg L (1991) The Consortium to Establish a Registry for Alzheimer's Disease (CERAD). Part II. Standardization of the neuropathologic assessment of Alzheimer's disease. Neurology 41:479–486

19. Nelson PT, Alafuzoff I, Bigio EH, Bouras C, Braak H, Cairns NJ, Castellani RJ, Crain BJ, Davies P, Del Tredici K et al (2012) Correlation of Alzheimer disease neuropathologic changes with cognitive status: a review of the literature. J Neuropathol Exp Neurol 71:362–381. doi:10.1097/NEN.0b013e31825018f7

20. Perez-Nievas BG, Stein TD, Tai HC, Dols-Icardo O, Scotton TC, Barroeta-Espar I, Fernandez-Carballo L, de Munain EL, Perez J, Marquie M et al (2013) Dissecting phenotypic traits linked to human resilience to Alzheimer's pathology. Brain J Neurol 136:2510–2526. doi:10.1093/brain/awt171

21. Pontecorvo MJ, Devous MD Sr, Navitsky M, Lu M, Salloway S, Schaerf FW, Jennings D, Arora AK, McGeehan A, Lim NC et al (2017) Relationships between flortaucipir PET tau binding and amyloid burden, clinical diagnosis, age and cognition. Brain J Neurol. doi:10.1093/brain/aww334

22. Qian J, Hyman BT, Betensky RA (2017) Neurofibrillary tangle stage and the rate of progression of Alzheimer symptoms: modeling using an autopsy cohort and application to clinical trial design. JAMA Neurol. doi:10.1001/jamaneurol.2016.5953

23. Riley KP, Snowdon DA, Markesbery WR (2002) Alzheimer's neurofibrillary pathology and the spectrum of cognitive function: findings from the Nun Study. Ann Neurol 51:567–577. doi:10.1002/ana.10161

24. Rosen C, Hansson O, Blennow K, Zetterberg H (2013) Fluid biomarkers in Alzheimer's disease—current concepts. Mol Neurodegener 8:20. doi:10.1186/1750-1326-8-20

25. Rowe CC, Ng S, Ackermann U, Gong SJ, Pike K, Savage G, Cowie TF, Dickinson KL, Maruff P, Darby D et al (2007) Imaging beta-amyloid burden in aging and dementia. Neurology 68:1718–1725. doi:10.1212/01.wnl.0000261919.22630.ea

26. Sander K, Lashley T, Gami P, Gendron T, Lythgoe MF, Rohrer JD, Schott JM, Revesz T, Fox NC, Arstad E (2016) Characterization of tau positron emission tomography tracer [18F]AV-1451 binding to postmortem tissue in Alzheimer's disease, primary tauopathies, and other dementias. Alzheimer's Dement J Alzheimer's Assoc 12:1116–1124. doi:10.1016/j.jalz.2016.01.003

27. Scholl M, Lockhart SN, Schonhaut DR, O'Neil JP, Janabi M, Ossenkoppele R, Baker SL, Vogel JW, Faria J, Schwimmer HD et al (2016) PET imaging of tau deposition in the aging human brain. Neuron 89:971–982. doi:10.1016/j.neuron.2016.01.028

28. Schwarz AJ, Yu P, Miller BB, Shcherbinin S, Dickson J, Navitsky M, Joshi AD, Devous MD Sr, Mintun MS (2016) Regional profiles of the candidate tau PET ligand 18F-AV-1451 recapitulate key features of Braak histopathological stages. Brain J Neurol. doi:10.1093/brain/aww023

29. Serrano-Pozo A, Frosch MP, Masliah E, Hyman BT (2011) Neuropathological alterations in Alzheimer disease. Cold Spring Harb Perspect Med 1:a006189. doi:10.1101/cshperspect.a006189

30. Smith R, Scholl M, Honer M, Nilsson CF, Englund E, Hansson O (2017) Tau neuropathology correlates with FDG-PET, but not AV-1451-PET, in progressive supranuclear palsy. Acta Neuropathol 133:149–151. doi:10.1007/s00401-016-1650-1

31. Villemagne VL, Ong K, Mulligan RS, Holl G, Pejoska S, Jones G, O'Keefe G, Ackerman U, Tochon-Danguy H, Chan JG et al (2011) Amyloid imaging with (18)F-florbetaben in Alzheimer disease and other dementias. J Nucl Med Off Publ Soc Nucl Med 52:1210–1217. doi:10.2967/jnumed.111.089730

32. Vonsattel JP, Del Amaya MP, Keller CE (2008) Twenty-first century brain banking. Processing brains for research: the Columbia University methods. Acta Neuropathol 115:509–532. doi:10.1007/s00401-007-0311-9

33. Wang L, Benzinger TL, Su Y, Christensen J, Friedrichsen K, Aldea P, McConathy J, Cairns NJ, Fagan AM, Morris JC et al (2016) Evaluation of tau imaging in staging Alzheimer disease and revealing interactions between beta-amyloid and tauopathy. JAMA Neurol. doi:10.1001/jamaneurol.2016.2078

34. Xia CF, Arteaga J, Chen G, Gangadharmath U, Gomez LF, Kasi D, Lam C, Liang Q, Liu C, Mocharla VP et al (2013) [(18)F] T807, a novel tau positron emission tomography imaging agent for Alzheimer's disease. Alzheimer's Dement J the Alzheimer's Assoc 9:666–676. doi:10.1016/j.jalz.2012.11.008